Crystallization and Chain Conformation of Semicrystalline and Amorphous Polymer Blends Studied by Wide-Angle and Small-Angle Scattering

CHING-I HUANG, JUN-RONG CHEN

Materials Science and Technology Program, Graduate Institute of Engineering Technology, National Taiwan University of Science and Technology, Taipei 106, Taiwan

Received 16 May 2001; revised 17 July 2001; accepted 21 August 2001

ABSTRACT: We examine the crystallization and chain conformation behavior of semicrystalline poly(ethylene oxide) (PEO) and amorphous poly(vinyl acetate) (PVAc) mixtures with wide-angle X-ray diffraction (WAXD), small-angle X-ray scattering (SAXS), and small-angle neutron scattering (SANS) experiments. For blends with PEO weight fractions (wt_{PEO}) greater than or equal to 0.3, below the melting point of PEO, the WAXD patterns reveal that crystalline PEO belongs to the monoclinic system. The unit-cell parameters are independent of wt_{PEO}. However, the bulk crystallinity determined from WAXD decreases as wt_{PEO} decreases. The scattered intensities from SAXS experiments show that the systems form an ordered crystalline/amorphous lamellar structure. In a combination of WAXD and SAXS analysis, the related morphological parameters are assigned correctly. With the addition of amorphous PVAc, both the average amorphous layer thickness and long spacing increase, whereas the average crystalline layer thickness decreases. We find that a two-phase analysis of the correlation function from SAXS, in which the scattering invariant is linearly proportional to the volume fraction of lamellar stacks, describes quantitatively the crystallization behavior of PEO in the presence of PVAc. When wt_{PEO} is close to 1, the samples are fully spaced-filled with lamellar stacks. As wt_{PEO} decreases from 1.0 to 0.3, more PVAc chains are excluded from the interlamellar region into the interfibrillar region. The fraction outside the lamellar stacks, which is completely occupied with PVAc chains, increases from 0 to 58%. Because the radius of gyration of PVAc with a random-coil configuration determined from SANS is smaller than the average amorphous layer thickness from SAXS, we believe that the amorphous PVAc chains still persist with a random-coil configuration even when the blends form an ordered structure. J Polym Sci Part B: Polym Phys 39: 2705–2715, 2001

Keywords: crystallization; chain conformation; wide-angle X-ray diffraction (WAXD); SAXS; small-angle neutron scattering (SANS); blends

INTRODUCTION

The phase behavior of crystalline polymer blends has attracted a lot of attention over the years. Much of the research has focused on crystalline/amorphous binary polymer blends.[1–16] For blends with at least one crystallizable component, most studies have been concerned with the morphology associated with the crystallization behavior. Much of the interest lies in the location of the amorphous polymer in the microstructure and the factors that influence the morphology development, such as the mobility and immiscibility be-

Correspondence to: C.-I. Huang (E-mail: chingi@mail.ntust.edu.tw)

Journal of Polymer Science: Part B: Polymer Physics, Vol. 39, 2705–2715 (2001)

tween the crystalline and amorphous components.[11] However, the chain conformation of each component, which plays a very important role in determining the location of each component and the morphological patterns, has not been fully understood.[3,16] In this article, we study both the chain conformation and crystallization behavior of semicrystalline and amorphous polymer mixtures. In particular, the effects of the addition of an amorphous polymer and temperature are examined.

We consider a model system of semicrystalline poly(ethylene oxide) (PEO) and amorphous poly(vinyl acetate) (PVAc). The melting point of PEO is around 60 °C. It is well known that PEO and PVAc are miscible over a wide range of temperatures and polymer compositions.[1,4–6,8–12] Although there have been some studies concerned with the microstructure of PEO/PVAc blends associated with the crystallization of PEO, most of them were examined with small-angle X-ray scattering (SAXS) experiments.[11] However, the controversy over the SAXS analysis with the correlation function[17] and the interphase distribution function[18–20] lies in the determination of the correct morphological parameters (crystalline layer thickness and amorphous layer thickness). Therefore, we employ both wide-angle X-ray diffraction (WAXD) and SAXS methods to probe the crystallization behavior of PEO in the presence of PVAc. This combination of WAXD and SAXS has been shown to be more appropriate in the analysis of morphological patterns that associate with the crystallization process.[21]

From the WAXD analysis, both the crystal structure and bulk crystallinity (ω_{mc}) are determined. From the one-dimensional (1D) correlation function via the SAXS analysis, two thickness parameters (L_1 and L_2) are obtained. In a comparison of ω_{mc}, $L_1/(L_1 + L_2)$, and $L_2/(L_1 + L_2)$, the average crystalline layer thickness and the average amorphous layer thickness can be assigned correctly. In addition, we compare the scattering invariant determined by both experiment and calculation, from which the fraction of lamellar stacks in the material and the location of both PEO and PVAc components can be determined quantitatively. Thus far, there have been no studies that analyze the morphological patterns of PEO/PVAc blends with a combination of WAXD and SAXS. We also employ small-angle neutron scattering (SANS) experiments to study the chain conformation of PEO/PVAc mixtures. In particular, we determine the net interaction parameter (χ), which is characteristic of the incompatibility between PEO and PVAc, and the radii of gyration of PEO and PVAc as a function of temperature and composition.

EXPERIMENTAL

Materials and Sample Preparation

The samples used in this study were mixtures of PEO and PVAc. PVAc with a molecular weight of 113,000 was purchased from Aldrich Chemical Co. PEO was purchased from Acros Organics Co. and had a molecular weight of 100,000. The mixtures were prepared by solution casting from chloroform at room temperature. The resulting films were evaporated in air at room temperature for 2 days and then under vacuum at 90 °C for 6 h to ensure complete solvent removal. The cast films were cut and compressed into Cu-window sample cells. The specimens were then kept at 90 °C in the oven to remove bubbles and voids. The samples were rapidly transferred to another oven preheated to 50 °C and were allowed to crystallize for 24 h.

WAXD

WAXD experiments were carried out on the blend samples with a Rigaku Denki diffractometer with Cu Kα radiation (λ = 1.542 Å) at a scanning rate of 1° θ/min, where θ is the scattering angle (the angle between the incident X-ray beam and the scattered X-ray beam). The accelerating voltage was 40 kV, and the tube current was 100 mA. The X rays were monochromated with a graphite. All measurements were performed at room temperature.

SAXS

SAXS experiments were carried out at National Tsing Hua University (Hsin-Chu, Taiwan). Cu Kα X rays (λ = 1.542 Å) were generated from an 18Kw Rigaku rotating anode. The power source was operated at 200 mA and 40 kV. The X rays were monochromated with graphite. Collimation of the X-ray beam was achieved with a set of three pinholes. The sizes of the first and second pinholes were 1.5 and 1.0 mm, respectively, and the size of the guard pinhole before the sample was 2.0 mm. The scattered intensity was collected by a two-dimensional position-sensitive detector (20

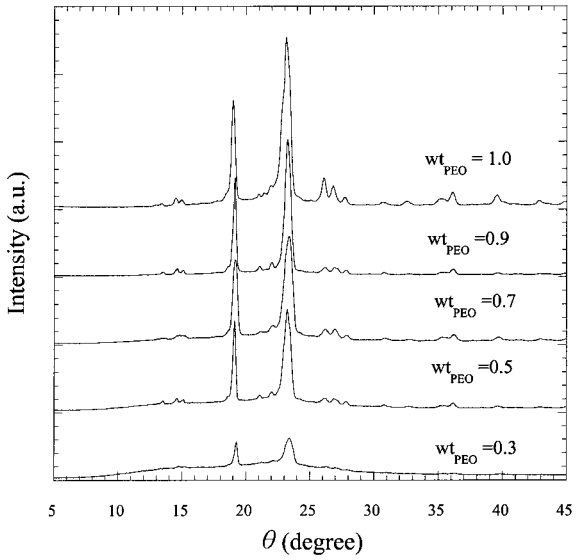

Figure 1. WAXD patterns in terms of the intensity and θ for the PEO/PVAc blends with various values of wt_{PEO} crystallized at 50 °C for 24 h.

$\times$ 20 cm^2) with approximately 1-mm resolution. The sample-to-detector distance was 2.27 m. The beam stop was a round lead disk 18 mm in diameter. The data were corrected for background and detector response and then azimuthally averaged to the 1D form of the intensity (I) versus the scattering wavevector [$q = (4\pi/\lambda)\sin(\theta/2)$]. All measurements were performed at room temperature.

SANS

SANS experiments were performed at the Cold Neutron Research Facility of the National Institute of Standards and Technology (United States) with the SANS 8m instrument. A wavelength λ of 9 Å was used. The sample-to-detector distance was 3.6 m. First, the blends were crystallized at 50 °C for 24 h and measured at room temperature. The samples were then heated and equilibrated at the desired temperature at least 20 min before measurement. In addition to the blend samples, SANS measurements were carried out on the pure homopolymers to estimate the incoherent background.

The scattering data were corrected for detector sensitivity, transmission, background, sample thickness, and empty cell contributions. The data were placed on an absolute scale with a calibrated silica standard (A3) and then azimuthally averaged. An incoherent scattered intensity from the homopolymer contributions was subtracted from the data. A small positive scattering intensity due to other uncertainties was removed. This magnitude was very small and typically about 0.1 cm^{-1}, which was within the experimental error.

RESULTS AND DISCUSSION

Crystallization Behavior

WAXD Analysis

The WAXD patterns in terms of I and θ for PEO/PVAc blends with various values of the PEO weight fraction (wt_{PEO}) crystallized at 50 °C for 24 h are shown in Figure 1. It is clear that the peak positions from the WAXD profiles are almost identical, which indicates that the crystallizable PEO chains form a similar unit-cell structure for the blends studied here. The peak positions from our blend samples in Figure 1 are consistent with those from ref. 22, indicating that PEO belongs to the monoclinic crystal system.[23] To analyze the unit-cell structure parameters, we have indexed the main peaks as suggested in ref. 22. For example, in Figure 2(a), five of the main peaks are indexed for the WAXD pattern from a pure PEO sample. For a monoclinic system, the interplanar spacing of the (hkl) reflection planes is given by

$$\left(\frac{1}{d_{hkl}}\right)^2 = \left(\frac{2\sin(\theta_{hkl}/2)}{\lambda}\right)^2 = \frac{1}{\sin^2\beta}\left(\frac{h^2}{a^2} + \frac{k^2\sin^2\beta}{b^2} + \frac{l^2}{c^2} - \frac{2hl\cos\beta}{ac}\right) \quad (1)$$

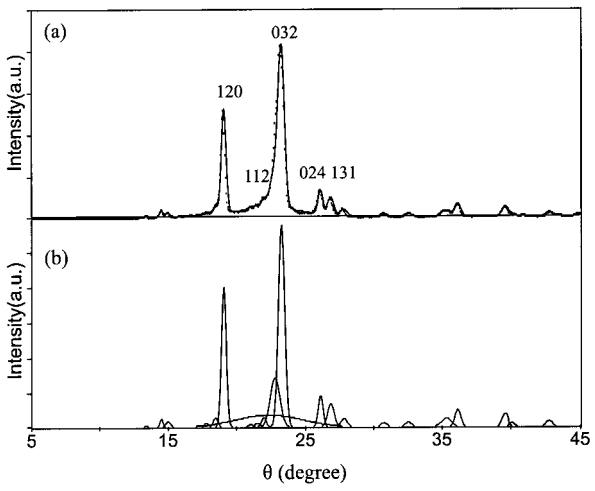

Figure 2. (a) WAXD pattern and (b) peak deconvolution of the WAXD profile for a pure PEO sample.

Table I. Unit-Cell Structure Parameters of PEO Crystals in the Presence of PVAc as Determined from WAXD Measurements

wt_{PEO}	a (Å)	b (Å)	c (Å)
1.0	8.13	13.13	19.58
0.9	8.11	13.05	19.64
0.7	8.10	13.00	19.56
0.5	8.11	13.05	19.64
0.3	8.02	13.00	19.41

Through the insertion of the values of λ (1.542 Å), β (125.4°, as in ref. 22), and the peak positions of (120), (032), and (024) reflection planes, the unit-cell parameters a, b, and c are determined by eq 1 and listed as a function of wt_{PEO} in Table I. As shown in Table I, the unit-cell parameters are independent of wt_{PEO}. That is, the crystal unit-cell structure of PEO remains the same with the addition of amorphous PVAc. However, the PVAc amount added to PEO has a great influence on the crystallinity of blend samples.

ω_{mc} for PEO, as determined from WAXD, is calculated by the division of the sum of the crystalline reflection intensities by the total intensity. By deconvoluting the WAXD profiles to a combination of possible crystalline reflections as well as the amorphous phase with Gaussian curves, we separate the intensities contributed from each crystalline reflection plane as well as the amorphous phase. For example, the WAXD deconvolution results from pure PEO samples are presented in Figure 2(b). All of the reflection planes as well as the corresponding θ values used in the deconvolution procedure for pure PEO are listed in Table II. The θ values with respect to (hkl) planes are calculated by the insertion of the unit-cell parameters into eq 1. Similar procedures are employed for the blend samples examined here. In Figure 3, we plot ω_{mc} versus wt_{PEO}. As expected, when wt_{PEO} decreases, ω_{mc} decreases.

Table II. Reflection Planes and Corresponding θ Values Used in the Deconvolution Procedure for PEO

h	k	l	θ (°)	h	k	l	θ (°)
1	0	0	13.4	0	3	2	23.2
0	2	1	14.6	0	2	4	26.1
1	1	0	15.0	1	3	1	26.7
0	1	3	18.0	1	1	3	27.8
1	1	1	18.5	2	0	1	30.6
1	2	0	19.0	1	1	4	32.9
0	3	1	21.0	1	4	2	35.1
0	2	3	21.5	1	2	−7	36.1
1	2	1	21.9	2	0	3	39.5
1	1	2	22.9	−1	4	−4	42.6

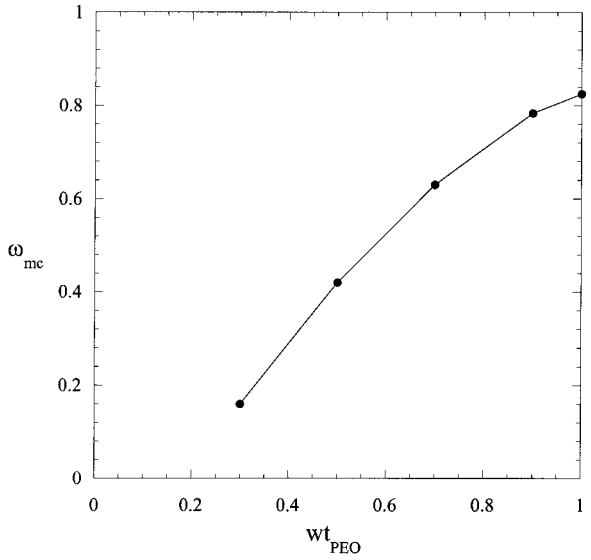

Figure 3. ω_{mc} determined from WAXD measurements as a function of wt_{PEO}.

SAXS Analysis

The SAXS intensity profiles are corrected by the subtraction of the background intensity arising from the thermal density fluctuation (I_b) with the aid of Porod–Ruland model:[24]

$$I(q) = K\frac{\exp(-\sigma^2 q^2)}{q^4} + I_b \qquad (2)$$

where K is the Porod constant and σ is related to the thickness of crystalline/amorphous interphases. The values of K, σ, and I_b are obtained by the curve fitting of the intensity at a high q range (0.10–0.15 $Å^{-1}$). A series of Lorentz-corrected scattering profiles [$(I - I_b)q^2$ vs q] obtained from SAXS experiments for PEO/PVAc blends crystallized at 50 °C for 24 h are shown in Figure 4. As can be seen, the peak position (q^*) shifts toward smaller scattering wavevectors with a decreasing amount of PEO. That is, the long spacing calculated from Bragg's law ($L_B = 2\pi/q^*$), as listed in Table III, increases with the addition of amorphous PVAc.

To obtain the average crystalline layer thickness (L_C) and average amorphous layer thickness

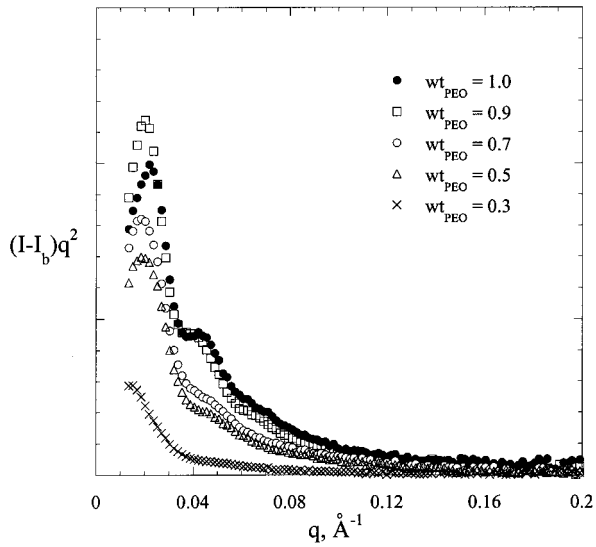

Figure 4. Profiles of the Lorentz-corrected intensity from SAXS measurements for PEO/PVAc blends crystallized at 50 °C (wt_{PEO} is indicated in the figure).

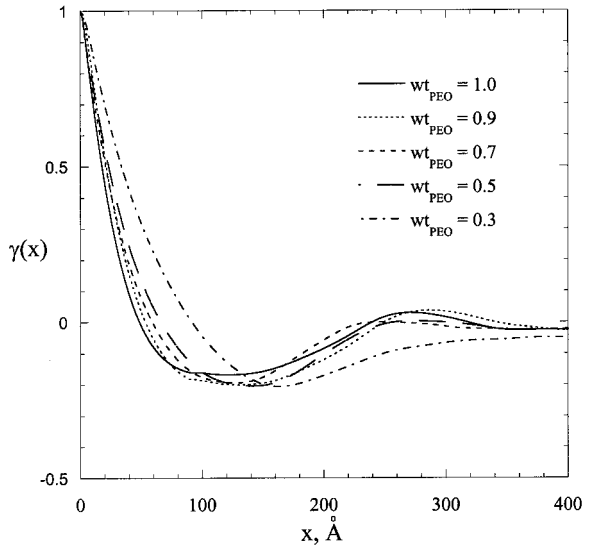

Figure 5. 1D correlation functions deduced from SAXS profiles of PEO/PVAc blends crystallized at 50 °C (wt_{PEO} is indicated in the figure).

(L_A), the normalized 1D correlation function [$\gamma(x)$], defined as[17]

$$\gamma(x) = \frac{1}{Q} \times \left\{ \frac{1}{2\pi^2} \int_0^\infty (I(q) - I_b) q^2 \cos(qx)\, dq \right\} \quad (3)$$

needs to be evaluated. In eq 3, the scattering invariant (Q) is defined as $\frac{1}{2\pi^2} \int_0^\infty [I(q) - I_b] q^2\, dq$. As a result, the correlation function becomes 1 at $x = 0$. Because the experimentally accessible q range is finite, the extrapolation of the scattered intensity to both low q and high q is necessary. The extension to high q data is performed as mentioned previously in eq 2. The extrapolation to zero q data is obtained by the curve fitting of the intensity at a low q range (0.013–0.03 $Å^{-1}$) with the Debye–Bueche model:[25,26]

$$I(q) = \frac{I(0)}{(1 + q^2\xi^2)^2} \quad (4)$$

where ξ is the correlation length. Once the extrapolations to both high q and low q range data are done, $\gamma(x)$ is calculated with eq 3. The value of the long spacing is, therefore, estimated as (1) the first maximum (L_{1D}^M) and (2) twice the position of the first minimum (L_{1D}^m) in the 1D correlation function $\gamma(x)$. The value L_{1D}^M corresponds to the most probable distance between two adjacent crystals, whereas $L_{1D}^m/2$ represents the most probable distance between a crystal and its adjacent amorphous layer region. In general, L_{1D}^M and L_{1D}^m do not coincide unless the lamellae form an ideal two-phase structure. In addition, the linear crystallinity (X_{CL}) is determined by

$$B = X_1(1 - X_1)L_{1D}^M \quad (5)$$

where B is the position of the first intercept of the correlation function $\gamma(x)$ with the x axis. In eq 5, either X_1 or $1 - X_1$ corresponds to $X_{CL} = L_C/L_{1D}^M$, from which L_C and $L_A = L_{1D}^M - L_C$ can be determined.

In Figure 5, we plot $\gamma(x)$ for wt_{PEO} = 1.0, 0.9, 0.7, 0.5, and 0.3, from which B, L_{1D}^M, and L_{1D}^m are determined and listed in Table III. We then ob-

Table III. Morphological Parameters Determined from Bragg's Law and 1D Correlation Functions for Blends of PEO and PVAc Crystallized at 50 °C for 24 h

wt_{PEO}	L_B (Å)	B (Å)	L_{1D}^M (Å)	L_{1D}^m (Å)	L_C (Å)	L_A (Å)
1.0	270	45	278	244	222	56
0.9	300	50	297	260	233	64
0.7	334	58	290	260	210	80
0.5	349	66	290	280	188	102
0.3	449	90	382	326	145	237

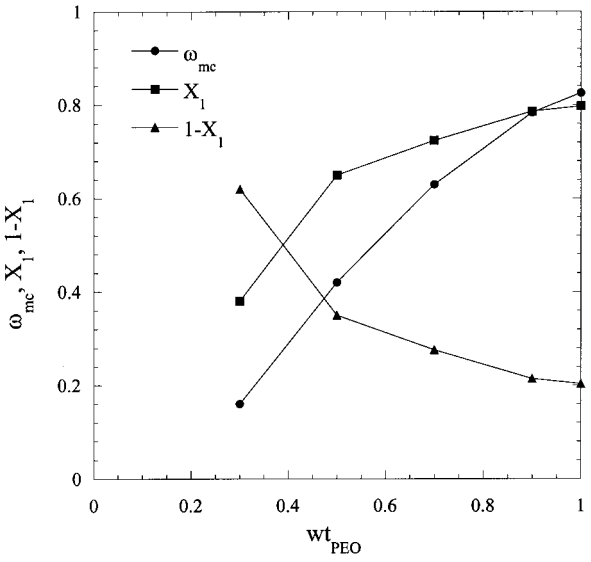

Figure 6. Variations of X_{CL} (X_1 or $1 - X_1$) determined from SAXS measurements and ω_{mc} determined from WAXD measurements.

tain two solutions, X_1 and $1 - X_1$, with eq 5. To distinguish whether X_1 or $1 - X_1$ represents X_{CL}, we present X_1, $1 - X_1$, and ω_{mc} from WAXD as a function of wt_{PEO} in Figure 6. As can be seen, if we assign the lower value $1 - X_1$ as X_{CL}, it would suggest that the volume fraction of lamellar stacks ($X_L = \omega_{mc}/X_{CL}$) is greater than 100% for $wt_{PEO} \geq 0.5$, which does not make sense. Therefore, it is reasonable to designate X_1 as X_{CL}. Note that when $wt_{PEO} = 1.0$, although $X_L = 1.03$, which is still greater than 1.0, the exceeding percentage 3% is within experimental error. Once X_{CL} is clearly identified, both L_C and L_A are determined and given in Table III. In Figure 7, we also plot the long spacing (L_B, L_{1D}^M, and L_{1D}^m), L_C, and L_A as a function of wt_{PEO}. As expected, both L_B and L_{1D}^m increase with an increasing amount of amorphous PVAc, whereas L_{1D}^M remains in the range of 278–297 Å as wt_{PEO} varies from 1.0 to 0.5 and then increases abruptly to 382 Å as wt_{PEO} decreases to 0.3. As the amount of amorphous PVAc increases, L_A increases; however, L_C decreases slightly. In general, we find that $L_B > L_{1D}^M > L_{1D}^m$, which suggests that there exists a broad distribution of long periods for the blend samples with $wt_{PEO} \geq 0.3$ crystallized at 50 °C.[18] Furthermore, as Santa-Cruz et al.[18] proposed, the inequality $L_{1D}^M > L_{1D}^m$ holds when the thicker phase has a broader distribution of sizes than the thinner phase. In a comparison of L_C and L_A in Table III, when $wt_{PEO} \geq 0.5$, the thicker phase corresponds to the crystalline lamellae, which is, therefore, characterized by a broader distribution of sizes than the amorphous phase. However, when wt_{PEO} is down to 0.3, the thinner phase corresponds to the crystalline lamellae, which has a narrower distribution of sizes than the amorphous phase.

Because X_{CL} (X_1 in our case) and ω_{mc} have been determined from SAXS and WAXD, respectively, the fraction of lamellar stacks occupied in the material (X_L) is easily calculated by $X_L = \omega_{mc}/X_{CL}$ and plotted as a function of wt_{PEO} in Figure 8. We find that when wt_{PEO} decreases from 1.0 to 0.3, X_L decreases from 100 to 42%. This indicates that as the amount of PVAc added to PEO increases, more PVAc chains are excluded from the interlamellar region into the interfibrillar region. Therefore, X_L decreases as wt_{PEO} decreases. These results have been observed qualitatively for A and B blends with the interaction parameter between A and B (χ_{AB}) close to 0.[3,11]

To further quantify the fraction of PEO in the crystalline and amorphous phases and the volume fraction of PVAc inside and outside the interlamellar stacks, we give a more detailed analysis by comparing both experimental and calculated values of Q, which is often written as[27]

$$Q = X_L X_{CL}(1 - X_{CL})(\rho_C - \rho_A)^2 \qquad (6)$$

where ρ_C and ρ_A are the scattering length densities of the crystalline layer and amorphous layer,

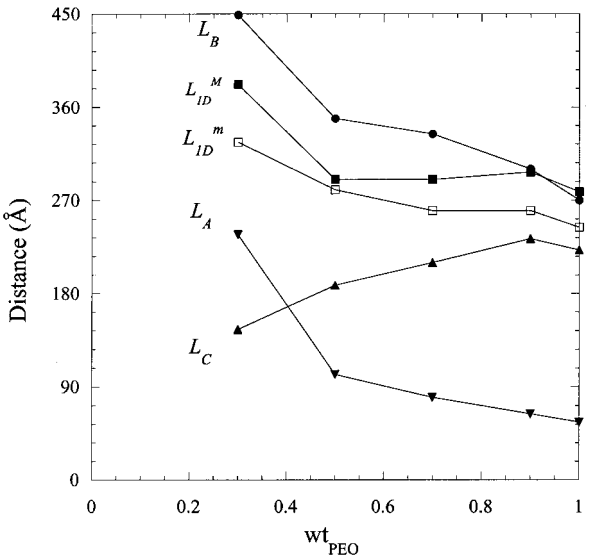

Figure 7. Long spacing deduced from Bragg's law (L_B) and 1D correlation functions (L_{1D}^M and L_{1D}^m) along with L_C and L_A from 1D correlation functions as a function of wt_{PEO}.

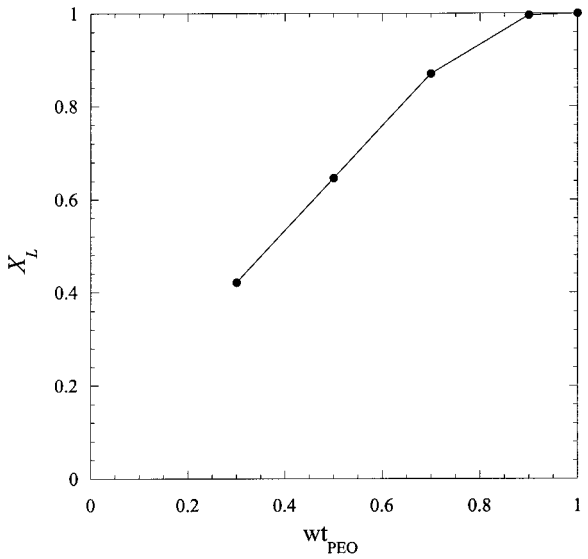

Figure 8. X_L in the bulk as a function of wt_{PEO}.

respectively. We assume that all of the PEO chains and partial amounts of the PVAc chains remain in the lamellar stacks. That is, the region outside the lamellar stacks $(1 - X_L)$ is fully occupied with amorphous PVAc. If ϕ_{PVAc} is denoted as the volume fraction of amorphous PVAc, the volume fraction of PVAc remaining outside and inside the lamellar stacks is, therefore, equal to $\phi_{PVAc,out} = 1 - X_L$ and $\phi_{PVAc,in} = \phi_{PVAc} - (1 - X_L)$, respectively. ρ_C and ρ_A are then represented as

$$\rho_C = \rho^{\circ}_{PEO,C} \tag{7a}$$

$$\rho_A = \rho^{\circ}_{PEO,A} \times \frac{\phi_{PEO,A}}{\phi_{PEO,A} + \phi_{PVAc} - (1 - X_L)} + \rho^{\circ}_{PVAc} \times \frac{\phi_{PVAc} - (1 - X_L)}{\phi_{PEO,A} + \phi_{PVAc} - (1 - X_L)} \tag{7b}$$

where $\phi_{PEO,A}$ represents the volume fraction of amorphous PEO, and $\rho^{\circ}_{PEO,C}$, $\rho^{\circ}_{PEO,A}$, and ρ°_{PVAc}, corresponding to the scattering length densities of 100% crystalline PEO, 100% amorphous PEO, and PVAc, respectively, are calculated by

$$\rho^{\circ}_I = \frac{b_I \times d^{\circ}_I}{(mw)_I} \times N_o \tag{8}$$

where $(mw)_I$ is the molecular weight of monomer I, N_o is Avogadro's number, and b_I is the scattering length per monomer I. In eq 8, $d^{\circ}_{PEO,C}$, $d^{\circ}_{PEO,A}$, and d°_{PVAc} represent the mass densities of 100% crystalline PEO, 100% amorphous PEO, and PVAc and equal 1.24, 1.12, and 1.19 g/cm^3, respectively.[28] For the X-ray source, b_I is equal to the number of electrons per monomer multiplied by 0.282×10^{-12} cm. With the insertion of the related values into eq 8, $\rho^{\circ}_{PEO,C}$, $\rho^{\circ}_{PEO,A}$, and ρ°_{PVAc} are equal to 1.148×10^{11}, 1.037×10^{11}, and 1.081×10^{11} cm^{-2}, respectively. For eq 7, the variables $\phi_{PEO,A}$ and ϕ_{PVAc} are determined by

$$\phi_{PEO,A} = \frac{wt_{PEO}(1 - f_C)/d^{\circ}_{PEO,A}}{(wt_{PEO}f_C/d^{\circ}_{PEO,C} + wt_{PEO}(1 - f_C)/d^{\circ}_{PEO,A} + (1 - wt_{PEO})/d^{\circ}_{PVAc}} \tag{9a}$$

$$\phi_{PVAc} = \frac{(1 - wt_{PEO})/d^{\circ}_{PVAc}}{(wt_{PEO}f_C/d^{\circ}_{PEO,C} + wt_{PEO}(1 - f_C)/d^{\circ}_{PEO,A} + (1 - wt_{PEO})/d^{\circ}_{PVAc}} \tag{9b}$$

where f_C is the ratio of crystalline PEO to the overall PEO content and can be determined by ω_{mc} from WAXD and the volume fraction of crystalline PEO ($\phi_{PEO,C}$) being equated:

$$\omega_{mc} = \phi_{PEO,C} = \frac{wt_{PEO}f_C/d^{\circ}_{PEO,C}}{(wt_{PEO}f_C/d^{\circ}_{PEO,C} + wt_{PEO}(1 - f_C)/d^{\circ}_{PEO,A} + (1 - wt_{PEO})/d^{\circ}_{PVAc}} \tag{9c}$$

Once f_C is determined with eq 9c, Q is calculated by eq 6 as mentioned previously. All of the related data are listed in Table IV. To compare Q from both experiment and calculation, we need to rescale the experimental Q because it is in arbitrary units. As shown in Table IV, the ratio of the calculated scattering invariant to the experimental scattering invariant, Q_{cal}/Q_{exp}, is almost independent of wt_{PEO} except for $wt_{PEO} = 0.3$. We then rescale Q_{exp} by multiplying the average value Q_{cal}/Q_{exp}, which is around 20.7×10^{19} cm^{-4}, and compare both Q_{cal} and scaled Q_{exp} in Figure 9. It is clear that both experimental and numerical results for $wt_{PEO} \geq 0.5$ are within a 5% experimental error, which suggests that the model adopted here describes quantitatively the crystallization behavior of PEO in the presence of PVAc very well.

On the basis of the results from both experiment and calculation, we conclude that the formed structure of PEO and PVAc blends transforms from interlamellar morphology to interfi-

Table IV. Experimental and Calculated Data via a Combination of WAXD and SAXS for Blends of PEO and PVAc Crystallized at 50 °C for 24 h

wt_{PEO}	ω_{mc}	X_{CL}	X_L	f_C	$\phi_{PEO,A}$	ϕ_{PVAc}	$\phi_{PVAc,out}$	$\phi_{PVAc,in}$	Q_{cal} ($\times 10^{19}$ cm^{-4})	Q_{exp} (arbitrary units)	Q_{cal}/Q_{exp} ($\times 10^{19}$ cm^{-4})	Scaled Q_{exp} ($\times 10^{19}$ cm^{-4})
1.0	0.825	0.797	1.03	0.839	0.175	0	0	0	1.799	0.081	22.2	1.677
0.9	0.783	0.786	0.996	0.883	0.114	0.103	0.004	0.099	1.376	0.070	19.7	1.449
0.7	0.630	0.724	0.870	0.917	0.063	0.307	0.130	0.177	1.074	0.054	19.9	1.118
0.5	0.420	0.650	0.646	0.864	0.073	0.507	0.354	0.153	0.971	0.046	21.1	0.952
0.3	0.160	0.380	0.421	0.557	0.141	0.699	0.579	0.120	0.818	0.028	29.2	0.580

brillar morphology with the addition of amorphous PVAc. As the amount of PVAc added to PEO increases, although $\phi_{PVAc,in}$, as listed in Table IV, increases and then decreases, $\phi_{PVAc,out}$ keeps increasing from 0 to 58%. That is, more PVAc chains are excluded from the interlamellar region into the interfibrillar region with decreasing wt_{PEO}. In addition, we find that f_C is over 80% when $wt_{PEO} \geq 0.5$ and then drops to 56% as wt_{PEO} decreases to 0.3, as listed in Table IV.

The calculated invariant Q for the blends with $wt_{PEO} = 0.3$ is substantially overestimated, which we believe happens because as X_L decreases and the exclusion of amorphous PVAc becomes larger, the spherulite morphology becomes more open.[29] Therefore, blends of partial crystalline PEO in the presence of large amounts of amorphous PVAc cannot form densely packed lamellar stacks. As shown in Figure 5, the 1D correlation function $\gamma(x)$ becomes more diffuse. Hence, the mean-squared scattering length density difference between the crystalline layer and amorphous layer $(\rho_C - \rho_A)^2$ as well as Q should be smaller than the calculated values.

Chain Conformation Behavior

We employ SANS experiments to examine the chain conformation behavior for the blends with wt_{PEO} = 0.7, 0.5, and 0.3 from 50 to 70 °C. As shown in Figure 10, where we plot I versus q for wt_{PEO} = 0.5, I is stronger at 50 °C because the PEO chains crystallize and the blends form a

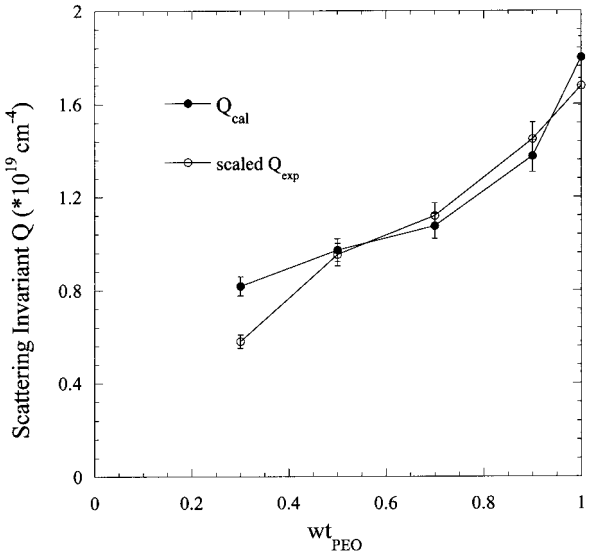

Figure 9. Comparison of Q_{cal} and Q_{exp} multiplied by the average ratio Q_{cal}/Q_{exp} (~20.7) for PEO/PVAc blends with various values of wt_{PEO} crystallized at 50 °C for 24 h.

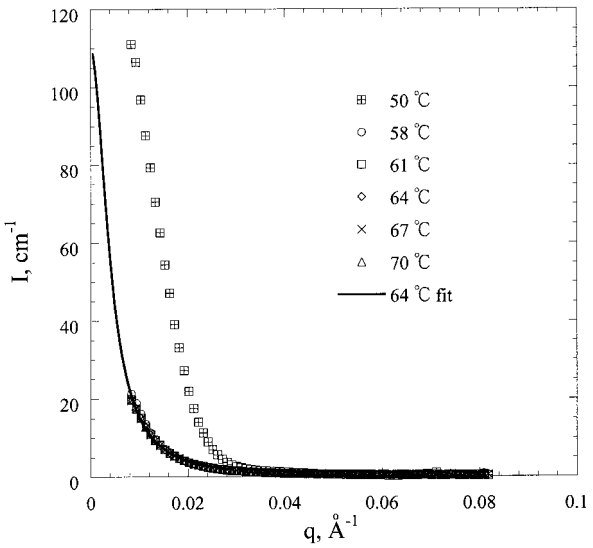

Figure 10. Scattered intensity $I(q)$ versus q from SANS measurements for wt_{PEO} = 0.5 PEO/PVAc blends at the indicated temperatures. The solid line is the best fit of the data at T = 64 °C to the RPA expression in eq 10.

Table V. Experimental Values of l^2_{ave}/v_o and χ/v_o for PEO/PVAc Systems from the Fitting of SANS Data to RPA in Eq 10

wt_{PEO}	ϕ_{PEO}	T (°C)	l^2_{ave}/v_o (Å^2/cm^3/mol)	χ/v_o ($\times 10^{-5}$; mol/cm^3)	$R_{g,PEO}$ (Å)	$R_{g,PVAc}$ (Å)
0.3	0.313	58	0.459	2.578	82.3	85.6
0.3	0.313	61	0.463	2.571	82.6	86.0
0.3	0.313	64	0.458	2.568	82.2	85.5
0.3	0.313	67	0.464	2.570	82.7	86.1
0.3	0.313	70	0.448	2.555	81.3	84.6
0.5	0.515	58	0.178	2.153	51.2	53.3
0.5	0.515	61	0.180	2.140	51.5	53.6
0.5	0.515	64	0.179	2.141	51.4	53.5
0.5	0.515	67	0.180	2.139	51.5	53.6
0.5	0.515	70	0.178	2.138	51.3	53.3
0.7	0.713	58	0.161	2.519	48.7	50.7
0.7	0.713	61	0.163	2.518	49.0	51.0
0.7	0.713	64	0.161	2.517	48.7	50.7
0.7	0.713	67	0.163	2.520	49.0	51.0
0.7	0.713	70	0.160	2.515	48.6	50.5

crystalline/amorphous periodic structure. As the temperature increases to 58 °C and even higher, the scattered intensity drops because the PEO chains melt and thus the ordered microstructures are destroyed. In fact, the melt-miscible PEO and PVAc chains are homogeneously mixed. Only the contrast between the randomly distributed PEO and PVAc chains contributes to the scattered intensity.

It is well known that the total scattering for a binary A and B mixture in the one-phase region is well described by random phase approximation (RPA):[30,31]

$$I(q) = N_o\left(\frac{b_A}{v_A} - \frac{b_B}{v_B}\right)^2 \times \left(\frac{1}{\phi_A Z_A v_A P_A(q)} + \frac{1}{\phi_B Z_B v_B P_B(q)} - 2\frac{\chi}{v_o}\right)^{-1} \quad (10)$$

where b_I is the scattering length per monomer I; v_I and v_o are the monomer volumes of the Ith segment and the reference unit, respectively; Z_I is the degree of polymerization of component I; ϕ_I is the volume fraction of component I and is calculated with densities of 1.12 and 1.19 g/cm^3 for 100% amorphous PEO and PVAc, respectively; and χ is the interaction parameter between components A and B. The single-chain form factor of component I, $P_I(q)$, is given by the Debye function:

$$P_I(q) = \frac{2}{x^2}[\exp(-x) - 1 + x], I = \text{A or B} \quad (11)$$

where $x = q^2R^2_{g,I}$, in which $R_{g,I}$ is the radius of gyration of component I.

The scattering data are fitted to eq 10 so that the values of the interaction parameter χ/v_o and the radii of gyration of PEO and PVAc, $R_{g,PEO}$ and $R_{g,PVAc}$, are obtained. Because $R_{g,PEO}$ and $R_{g,PVAc}$ are strongly coupled in eq 10, they cannot be varied independently. A single averaged parameter l^2_{ave}/v_o is introduced in the fitting procedure with[31]

$$R^2_{gI} = \frac{Z_I v_I}{6}\left(\frac{l^2_{ave}}{v_o}\right), I = \text{A or B} \quad (12)$$

Thus, only two independent parameters, l^2_{ave}/v_o and χ/v_o, exist in the fitting procedure. As shown in Figure 10, the scattered intensities for the blends with $wt_{PEO} = 0.5$ at $T \geq 58$ °C are well fitted by eq 10 for the whole q range. Similar results are obtained for $wt_{PEO} = 0.3$ and 0.7. Furthermore, the values of l^2_{ave}/v_o and χ/v_o obtained from the fits as a function of wt_{PEO} and temperature are given in Table V. It is clear that the interaction parameter χ/v_o is very small (close to zero) and independent of the volume fraction and temperature range studied here. In terms of l^2_{ave}/v_o, $R_{g,PEO}$ and $R_{g,PVAc}$ calculated from eq 12 are around 50–85 Å for $wt_{PEO} = 0.7$–0.3. From a comparison with L_A results obtained for systems crystallized at 50 °C (as shown in Table III), it is clear that the amorphous layer thickness is always larger than $R_{g,PVAc}$. As such, there is enough

space for the amorphous PVAc chains with a random-coil configuration.

SUMMARY

We have employed WAXD, SAXS, and SANS experiments to study the crystallization and chain conformation behavior of melt-miscible semicrystalline PEO and amorphous PVAc mixtures. From the WAXD analysis for the blends with $wt_{PEO} \geq 0.3$ quenched from the melt state to a temperature below the melting point of PEO, such as 50 °C, the crystalline PEO belongs to the monoclinic system, and the unit-cell parameters (a, b, c, and β) are independent of wt_{PEO}. However, ω_{mc} determined from WAXD decreases with an increasing amount of PVAc. SAXS results show that the mixtures quenched to 50 °C form an ordered crystalline/amorphous lamellar structure. In a combination of the results of ω_{mc} from WAXD and X_{CL} from SAXS, X_L (ω_{mc}/X_{CL}) is obtained. As wt_{PEO} decreases from 1.0 to 0.3, X_L decreases from 100 to 42%. Furthermore, we find that the scattering invariant deduced from the 1D correlation function follows the following expression: $Q = X_L X_{CL}(1 - X_{CL})(\rho_C - \rho_A)^2$. Our results from both experiment and calculation make clear that the structure of PEO and PVAc blends transforms from interlamellar morphology to interfibrillar morphology with the addition of amorphous PVAc. When wt_{PEO} is close to 1, the samples are fully spaced-filled with lamellar stacks. That is, the amorphous PVAc chains are located between the crystalline interlamellae. As the amount of PVAc added to PEO increases, more PVAc chains are excluded from the interlamellar region into the interfibrillar region. With the addition of amorphous PVAc, L_A, as well as the average long spacing, increases, whereas L_C decreases.

Although the PEO chains in the blend systems crystallize at 50 °C, once the systems are heated to around 58 °C, the formed lamellar structures disappear very quickly by melting. The scattering data from SANS experiments are well described by RPA, indicating that both the PEO and PVAc chains are randomly distributed over all length scales. In particular, the interaction parameter is very small (close to zero) and independent of wt_{PEO} and temperature, as expected. Because $R_{g,PVAc}$ with a random-coil configuration determined from SANS is smaller than L_A from SAXS for the blends with $wt_{PEO} \geq 0.3$, we believe that the amorphous PVAc chains still persist with a random-coil configuration even when the blends form an ordered structure.

The authors thank Dr. T. L. Lin and Dr. W. C. Liu for their assistance with the SAXS measurements and Dr. Charles C. Han for his assistance with the SANS 8m measurements. This work was supported by the National Science Council of the Republic of China (grant NSC 89-2216-E-011-019) and the Institute of Nuclear Energy Research of the Republic of China (grant 892001INER027).

REFERENCES AND NOTES

1. Martuscelli, E.; Silvestre, C.; Gismondi, C. Makromol Chem 1985, 186, 2161.
2. (a) Inaba, N.; Sato, K.; Suzuki, S.; Hashimoto, T. Macromolecules 1986, 19, 1690; (b) Inaba, N.; Sato, K.; Suzuki, S.; Hashimoto, T. Macromolecules 1988, 21, 407.
3. Ito, H.; Russell, T. P.; Wignall, G. D. Macromolecules 1987, 20, 2213.
4. Martuscelli, E.; Vicini, L.; Seves, A. Makromol Chem 1987, 188, 607.
5. Silvestre, C.; Karasz, F. E.; Macknight, W.; Martuscelli, E. Eur Polym J 1987, 23, 745.
6. Kalfoglou, N. K.; Sotiropoulou, D. D.; Margaritis, A. G. Eur Polym J 1988, 24, 389.
7. Burghardt, W. R. Macromolecules 1989, 22, 2482.
8. Addonozio, M. L.; Martuscelli, E.; Silvestre, C. J Polym Mater 1990, 7, 63.
9. Han, C. D.; Chung, H. S.; Kim, J. K. Polymer 1992, 33, 546.
10. Yin, J.; Alfonso, G. C.; Turturro, A.; Pedemonte, E. Polymer 1993, 34, 1465.
11. Talibuddin, S.; Wu, L.; Runt, J.; Lin, J. S. Macromolecules 1996, 29, 7527.
12. Chen, X.; Yin, J.; Alfonso, G. C.; Pedemonte, E.; Turturro, A.; Gattiglia, E. Polymer 1998, 39, 4929.
13. Chen, H. L.; Hsiao, M. S. Macromolecules 1998, 31, 6579.
14. Seki, M.; Nakano, H.; Yamauchi, S.; Suzuki, J.; Matsushita, Y. Macromolecules 1999, 32, 3227.
15. Lim, S. W.; Lee, K. H.; Lee, C. H. Polymer 1999, 40, 2837.
16. Huang, C. I. J Polym Res, in press.
17. Strobl, G. R.; Schneider, M. J Polym Sci Polym Phys Ed 1980, 18, 1343.
18. Santa Cruz, C. S.; Stribeck, N.; Zachmann, H. G.; Balta Calleja, F. J. Macromolecules 1991, 24, 5980.
19. Stribeck, N.; Alamo, R. G.; Mandelkern, L.; Zachmann, H. G. Macromolecules 1995, 28, 5029.
20. Albrecht, T.; Strobl, G. Macromolecules 1996, 29, 783.

21. Wang, Z. G.; Hsiao, B. S.; Fu, B. X.; Liu, L.; Yeh, F.; Sauer, B. B.; Chang, H.; Schultz, J. M. Polymer 2000, 41, 1791.
22. Marcos, J. I.; Orlandi, E.; Zerbi, G. Polymer 1990, 31, 1899.
23. Takahashi, Y.; Tadokoro, H. Macromolecules 1973, 6, 672.
24. Ruland, W. J. J Appl Crystallogr 1971, 4, 70.
25. Debye, P.; Bueche, A. M. J Appl Phys 1949, 20, 518.
26. Debye, P.; Anderson, H. R., Jr.; Brumberger, H. J Appl Phys 1957, 28, 679.
27. (a) Gehrke, R.; Riekel, C.; Zachmann, H. G. Polymer 1989, 30, 1582; (b) Kruger, K. N.; Zachmann, H. G. Macromolecules 1993, 26, 5202.
28. Brandrup, J.; Immerfrut, E. H. Polymer Handbook; Wiley: New York, 1989.
29. Saito, H.; Stuhn, B. Macromolecules 1994, 27, 216.
30. de Gennes, P. G. Scaling Concepts in Polymer Physics; Cornell University Press: Ithaca, NY, 1979.
31. Shibayama, M.; Yang, H.; Stein, R. S.; Han, C. C. Macromolecules 1985, 18, 2179.